The Dynamic Control of Reactive Power for the Brushless Doubly Fed Induction Machine With Indirect Stator-Quantities Control Scheme

Rongli Zhao, Ailing Zhang, Yun Ma, Xin Wang, Jun Yan, and Zhizhong Ma

***Abstract*—Compared to the doubly fed induction machine (DFIM), the brushless doubly fed induction machine (BDFIM) has higher reliability by virtue of the absence of a brush gear. Recent research on structure optimization design and control strategy of BDFIM has made remarkable progress. BDFIM indirect stator-quantities control (ISC) is a new control strategy, which, in comparison to vector control strategy, requires fewer parameters and does not need rotating coordinate transformation. This paper further develops the dynamic control of reactive power for the BDFIM with ISC scheme. Detailed theoretical analysis is done to show the controller structure of the reactive power. The experimental results of the prototype show the feasibility of the proposed scheme. As a result, the proposed ISC controllers have been able to control not only speed and torque, but also the reactive power.**

***Index Terms*—Brushless doubly fed induction machine (BDFIM), brushless doubly fed machine (BDFM), indirect stator-quantities control (ISC), reactive power control.**

I. Introduction

THE brushless doubly fed machine (BDFM) has been attractive, in recent years, in certain industrial applications for its intrinsic advantages of being brushless and its high reliability. BDFM has two three-phase windings in the stator: one is power winding (PW) connected directly to the power grid, the other is control winding (CW) fed by a converter. Each winding produces an air-gap field of a different pole number, chosen to avoid electromagnetic cross-coupling between the two stators. The rotor is specially designed to couple to both air-gap fields. There are two styles of rotor structure: reluctance rotor (brushless doubly fed reluctance machine, BDFRM) and nested cage rotor (brushless doubly fed induction machine, BDFIM). The sample machine used in this paper is BDFIM.

Manuscript received April 5, 2014; revised June 30, 2014 and September 13, 2014; accepted October 13, 2014. Date of publication October 29, 2014; date of current version April 15, 2015. This work was supported by the National Natural Science Foundation of China under Grant 50877051. Recommended for publication by Associate Editor B. Singh.

R. Zhao, A. Zhang, J. Yan, and Z. Ma are with the College of Electrical and Power Engineering, Taiyuan University of Technology, Taiyuan 030024, China (e-mail: zrl5663325@126.com; zallucy@126.com; mahouuu@163.com; mzzgxl@163.com).

Y. Ma was with the College of Electrical and Power Engineering, Taiyuan University of Technology, Taiyuan 030024, China He is now with the State Grid Jinzhong Power Supply Company, Jinzhong 030600, China. (e-mail: hswolf@163.com).

X. Wang was with the College of Electrical and Power Engineering, Taiyuan University of Technology, Taiyuan 030024, China. She is now with the CSR Zhuzhou Electric Company, Zhuzhou 412000, China (e-mail: lo.w@163.com).

Color versions of one or more of the figures in this paper are available online at http://ieeexplore.ieee.org.

Digital Object Identifier 10.1109/TPEL.2014.2365675

Compared to the doubly fed induction machine (DFIM), the BDFM retains the benefit of a low-cost converter. Moreover, due to the absence of a brush gear, the cost of maintenance is less than that of DFIM. Therefore, BDFM is better suited for operations requiring minimal maintenance such as wind power generation [1]. Recently, researches on structure optimization design and control strategy of BDFIM have become hot issues. In 2010, Ohio State University designed a 200-kW high efficiency BDFRM with energy efficiency higher than 96% [2]. In 2012, a research group at the University of Cambridge developed a 250-kW brushless doubly fed induction generator (BDFIG) and matched control system [3]. In the same year, the same group proposed a control strategy enabling the BDFIG to successfully ride through a symmetrical voltage dips [4] and implemented the control strategy on a 250-kW BDFIG. Their experimental results indicated that the low voltage ride through is possible without a crowbar. The BDFIM shows potential commercial promise in wind power generation based on results of the research.

Research of BDFIM control strategies have rapidly progressed since two-axis models [5]–[8] established in the 1990s, the majority of which have focused on vector control (VC) strategy and direct torque control (DTC) strategy. With respect to VC, Shao proposed PW flux-oriented VC strategy, which can be used to control both the speed and the reactive power [9], [10]. However, due to a lack of an inner current loop, there was no current-limit, and the dynamic performance was influenced significantly. Poza developed a new VC algorithm that allows control of the reactive power and speed, in which six PI regulators are required even if there is current-limit [11], [12]. Long and Tohidi improved the VC scheme presented in [9] and [10] to a new control scheme with an inner current loop and an outer voltage loop [4], [13], which was similar to VC scheme for DFIM. Even with the simplified structure of the BDFIM VC control and improved in performance, the rotating coordinate transformations still complicate the system structure in ways similar to traditional induction machine VC scheme.

The DTC strategy is a new control strategy applied successfully for induction machines [14] after the appearance of VC. Unlike VC, DTC does not require rotating coordinate transformations to achieve decoupled control of the flux linkage and torque, so its structure is simple. Sarasola *et al.* derived analytical expressions showing the viability of the DTC technique for a specific BDFIM design in two papers published in 2007 [15] and 2011 [16], respectively, but did not address the reactive power control issue. A control scheme for the torque and

reactive power of BDFRM was proposed by Hamza [17]. Similar to the DTC technique, a switching table that simultaneously satisfies the demands of controlling both torque and reactive power is presented, and although a control strategy is proposed, the exact expression of reactive power and CW flux linkage is not put forth in this paper. The control schemes involved in [15]–[17] all adopt the switching table conceptually similar to the induction machine's DTC strategy; therefore, the same disadvantages of larger current fluctuations in low frequency still exist in BDFM DTC strategy.

An indirect stator-quantities control (ISC) strategy for the BDFIM was proposed for the first time by Zhang *et al.* [18], [19]. In this strategy, complex rotating coordinate transformations are no longer required, so it can be implemented with a simple structure. The inner torque loop provides the capability of current-limit and improves dynamic performance. Moreover, ISC is less dependent on machine parameters, since only two stator winding resistances are needed. The experimental results of the prototype show the feasibility of the proposed strategy for the BDFIM. However, the dynamic control of the reactive power has not been discussed.

One of the advantages of BDFIM is that the reactive power can be regulated. When BDFIM acts as a motor, the power factor of the grid can be improved by controlling the reactive power. When employed as a generator, especially as a generator for wind generation, providing a certain amount of reactive power can support the voltage control at the point of common coupling. Moreover, reactive power control is one of the most common requirements for the wind farms in some grid codes [20]. So, the reactive power control strategy for BDFIM should be developed. This paper is an extension of the work presented in [19]. The relationship between PW reactive power and CW flux linkage is detailed here, and a design for the reactive power controller is presented. This will allow the ISC system to control not only speed and torque, but also the reactive power. All the work has been tested and validated in an experimental machine prototype.

II. BDFIM Mathematic Model

The BDFIM can be modeled with the following (1)–(6) flux and voltage equations in the CW static reference frame [8]:

$$\vec{\psi}_{\rm p} = L_{\rm p}\vec{i}_{\rm p} + L_{\rm hp}\vec{i}_{\rm r} \tag{1}$$

$$\vec{\psi}_{\rm c} = L_{\rm c}\vec{i}_{\rm c} + L_{\rm hc}\vec{i}_{\rm r} \tag{2}$$

$$\vec{\psi}_{\rm r} = L_{\rm hp}\vec{i}_{\rm p} + L_{\rm hc}\vec{i}_{\rm c} + L_{\rm r}\vec{i}_{\rm r} \tag{3}$$

$$\vec{u}_{\rm p} = R_{\rm p}\vec{i}_{\rm p} + \frac{d\vec{\psi}_{\rm p}}{dt} - j(p_{\rm p}+p_{\rm c})\omega_{\rm r}\vec{\psi}_{\rm p} \tag{4}$$

$$\vec{u}_{\rm c} = R_{\rm c}\vec{i}_{\rm c} + \frac{d\vec{\psi}_{\rm c}}{dt} \tag{5}$$

$$\vec{u}_{\rm r} = 0 = R_{\rm r}\vec{i}_{\rm r} + \frac{d\vec{\psi}_{\rm r}}{dt} - jp_{\rm c}\omega_{\rm r}\vec{\psi}_{\rm r}. \tag{6}$$

The PW reactive power referred to CW static reference frame can be expressed as follows (see Appendix I):

$$Q_{\rm p} = \frac{3}{2}{\rm Im}(\vec{i}_{\rm p}^{*}\vec{u}_{\rm p}) \tag{7}$$

where in (1)–(7) $\vec{i}$, $\vec{u}$, and $\vec{\psi}$ indicate current, voltage, and flux linkage vectors. The superscript $*$ expresses the complex conjugate of the vector. The subscript *p*, *c*, and *r* express the PW, CW, and rotor respectively, for example, $\vec{u}_{\rm p}$ is PW voltage vector. $R_{\rm p}$, $R_{\rm c}$, and $R_{\rm r}$ indicate resistance. $L_{\rm hp}$ and $L_{\rm hc}$ are the coupling-inductances between the PW, CW, and the rotor, and $L_{\rm p}$, $L_{\rm c}$, and $L_{\rm r}$ express self-inductance. *P* is pole-pair. $\omega_{\rm r}$ is the mechanical angular speed. It is worth noting that (1)–(7) are in the CW static reference frame; hence, all vectors rotate at the CW angular frequency. For example, in the steady state, $\vec{\psi}_{\rm c}$ can be expressed as

$$\vec{\psi}_{\rm c} = \left|\vec{\psi}_{\rm c}\right| e^{j\vec{\psi}_{\rm c}t} \tag{8}$$

where $\left|\vec{\psi}_{\rm c}\right|$ is the magnitude of $\vec{\psi}_{\rm c}$ and $\omega_{\rm c}$ is CW angular frequency.

Based on (1)–(6), an equivalent circuit is obtained as shown in Fig. 1, in which δ represents the differential operator *d/dt*.

III. Relationship Between PW Reactive Power and CW Flux Linkage

From (1), $\vec{i}_{\rm r}$ can be expressed as

$$\vec{i}_{\rm r} = \frac{1}{L_{hp}}\vec{\psi}_{\rm p} - \frac{L_{\rm p}}{L_{hp}}\vec{i}_{\rm p}. \tag{9}$$

Substituting (9) into (2), $\vec{i}_{\rm c}$ can be expressed as

$$\vec{i}_{\rm c} = \frac{1}{L_{\rm c}}\vec{\psi}_{\rm c} - \frac{L_{\rm hc}}{L_{\rm c}L_{\rm hp}}\vec{\psi}_{\rm p} + \frac{L_{\rm hc}L_{\rm P}}{L_{\rm c}L_{\rm hp}}\vec{i}_{\rm p}. \tag{10}$$

Substituting (9) and (10) into (3), eliminating $\vec{i}_{\rm r}$ and $\vec{i}_{\rm c}$, $\vec{\psi}_{\rm r}$ can be expressed as

$$\begin{aligned}\vec{\psi}_{\rm r} &= L_{\rm hp}\vec{i}_{\rm p} + L_{\rm hc}\vec{i}_{\rm c} + L_{\rm r}\vec{i}_{\rm r}\\ &= \frac{L_{\rm hc}}{L_{\rm c}}\vec{\psi}_{\rm r} + \frac{L_{\rm c}L_{\rm r} - L_{\rm hc}^2}{L_{\rm c}L_{\rm hp}}\vec{\psi}_{\rm p}\\ &\quad + \frac{L_{\rm c}I_{\rm hp}^2 + L_{\rm p}I_{\rm hc}^2 - L_{\rm c}L_{\rm p}L_{\rm r}}{L_{\rm c}L_{\rm hp}}\vec{i}_{\rm p}.\end{aligned} \tag{11}$$

Taking (9) and (11) into account, according to the Heaviside rules [21], replacing *d/dt* by differential operator δ, (6) can be derived into following:

$$\begin{aligned}0 &= R_{\rm r}\vec{i}_{\rm r} + (\delta - jp_{\rm c}\omega_{\rm r})\vec{\psi}_{\rm r}\\ &= \frac{R_{\rm r}}{\delta - jp_{\rm c}\omega_{\rm r}}\left(\frac{1}{L_{\rm hp}}\vec{\psi}_{\rm p} - \frac{L_{\rm p}}{L_{\rm hp}}\vec{i}_{\rm p}\right)\\ &\quad + \left(\frac{L_{\rm hc}}{L_{\rm c}}\vec{\psi}_{\rm c} + \frac{L_{\rm c}L_{\rm r} - L_{\rm hc}^2}{L_{\rm c}L_{\rm hp}}\vec{\psi}_{\rm p} + \frac{L_{\rm c}L_{\rm hp}^2 + L_{\rm p}L_{\rm hc}^2 - L_{\rm c}L_{\rm p}L_{\rm r}}{L_{\rm c}L_{\rm hp}}\vec{i}_{\rm p}\right)\\ &= \left(\frac{R_{\rm r}/L_{\rm hp}}{\delta - jp_{\rm c}\omega_{\rm r}} + \frac{L_{\rm c}L_{\rm r} - L_{\rm hc}^2}{L_{\rm c}L_{\rm hp}}\right)\vec{\psi}_{\rm p}\\ &\quad + \left(\frac{L_{\rm c}L_{\rm hp}^2 + L_{\rm p}L_{\rm hc}^2 - L_{\rm c}L_{\rm p}L_{\rm r}}{L_{\rm c}L_{\rm hp}} - \frac{R_{\rm r}L_{\rm p}/L_{\rm hp}}{\delta - jp_{\rm c}\omega_{\rm r}}\right)\vec{i}_{\rm p}\\ &\quad + \frac{L_{\rm hc}}{L_{\rm c}}\vec{\psi}_{\rm c}.\end{aligned} \tag{12}$$

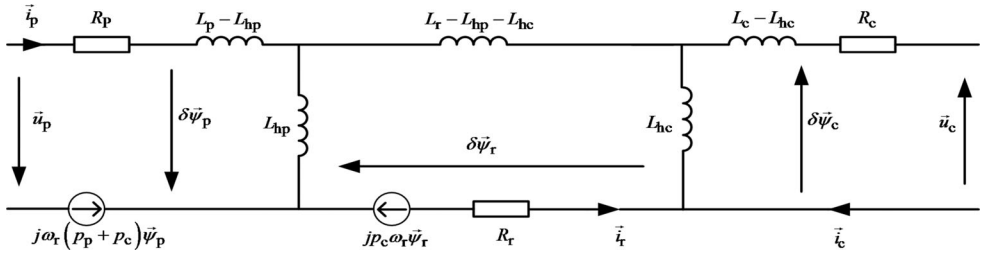

Fig. 1. Equivalent circuit for BDFIM.

Eq. (12) can be rewritten as

$$\left(\frac{R_{\rm r}L_{\rm p}/L_{\rm hp}}{\delta - jp_{\rm c}\omega_{\rm r}} - \frac{L_{\rm c}L_{\rm hp}^2 + L_{\rm p}L_{\rm hc}^2 - L_{\rm c}L_{\rm p}L_{\rm r}}{L_{\rm c}L_{\rm hp}}\right)\vec{i}_{\rm p} = \frac{L_{\rm hc}}{L_{\rm c}}\vec{\psi}_{\rm c} + \left(\frac{R_{\rm r}/L_{\rm hp}}{\delta - jp_{\rm c}\omega_{\rm r}} + \frac{L_{\rm c}L_{\rm r} - L_{\rm hc}^2}{L_{\rm c}L_{\rm hp}}\right)\vec{\psi}_{\rm p} \quad (13)$$

where δ can be replaced by $j\omega_{\rm c}$in the steady state. Whatever in steady state and transient, $\delta - jp_{\rm c}\omega_{\rm r}$ is very larger compared with other terms in (13), and its reciprocal can be neglected [4]. Therefore, (13) is simplified as

$$\frac{L_{\rm c}L_{\rm hp}^2 + L_{\rm p}L_{\rm hc}^2 - L_{\rm c}L_{\rm p}L_{\rm r}}{L_{\rm c}L_{\rm hp}}\vec{i}_{\rm p} = -\frac{L_{\rm hc}}{L_{\rm c}}\vec{\psi}_{\rm c} - \frac{L_{\rm c}L_{\rm r} - L_{\rm hc}^2}{L_{\rm c}L_{\rm hp}}\vec{\psi}_{\rm p}. \quad (14)$$

From (14), $\vec{i}_{\rm p}$ can be expressed in terms of $\vec{\psi}_{\rm c}$ and $\vec{\psi}_{\rm p}$

$$\vec{i}_{\rm p} = -\frac{L_{\rm hc}L_{\rm hp}\vec{\psi}_{\rm c} + (L_{\rm c}L_{\rm r} - L_{\rm hc}^2)\vec{\psi}_{\rm p}}{L_{\rm c}L_{\rm hp}^2 + L_{\rm p}L_{\rm hc}^2 - L_{\rm c}L_{\rm p}L_{\rm r}}. \quad (15)$$

In (4), ignoring resistance $R_{\rm p}$ voltage drop, the relation between $\vec{\psi}_{\rm p}$ and $\vec{u}_{\rm p}$ can be expressed as (See Appendix II)

$$\vec{\psi}_{\rm p} = \frac{1}{\omega_{\rm c}}\vec{u}_{\rm p}e^{j\frac{\pi}{2}}. \quad (16)$$

By substituting (15) and (16) into (7), the reactive power $Q_{\rm p}$ can be derived as

$$\begin{aligned} Q_{\rm p} &= \frac{3}{2}{\rm Im}(\vec{i}_{\rm p}^{*}\vec{u}_{\rm p}) \\ &= -\frac{3}{2}{\rm Im}\left(\frac{L_{\rm hc}L_{\rm hp}\vec{\psi}_{\rm c}^{*} + (L_{\rm c}L_{\rm r} - L_{\rm hc}^2)\vec{\psi}_{\rm p}^{*}}{L_{\rm c}L_{\rm hp}^2 + L_{\rm p}L_{\rm hc}^2 - L_{\rm c}L_{\rm p}L_{\rm r}}\right)\vec{u}_{\rm p} \\ &= -\frac{3}{2}{\rm Im}\left(\frac{L_{\rm hc}L_{\rm hp}\vec{\psi}_{\rm c}^{*} + (L_{\rm c}L_{\rm r} - L_{\rm hc}^2)\frac{1}{\omega_{\rm c}}\vec{u}_{\rm p^e}^{*-j\frac{\pi}{2}}}{L_{\rm c}L_{\rm hp}^2 + L_{\rm p}L_{\rm hc}^2 - L_{\rm c}L_{\rm p}L_{\rm r}}\right)\vec{u}_{\rm p} \\ &= -\frac{3}{2}A_1{\rm Im}\left[L_{\rm hc}L_{\rm hp}\vec{\psi}_{\rm c}^{*}\vec{u}_{\rm p} + A_2\frac{1}{\omega_{\rm c}}\vec{u}_{\rm p^e}^{*-{\rm j}\frac{\pi}{2}}\vec{u}_{\rm p}\right] \end{aligned} \quad (17)$$

where

$$A_1 = \frac{1}{L_{\rm c}L_{\rm hp}^2 + L_{\rm p}L_{\rm hc}^2 - L_{\rm c}L_{\rm p}L_{\rm r}}$$
$$A_2 = (L_{\rm c}L_{\rm r} - L_{\rm hc}^2).$$

As shown in (17), since the PW is connected to the grid and cannot be directly controlled, the PW reactive power is only relevant to the CW flux $\vec{\psi}_{\rm c}$. That is to say, control of the reactive power can be achieved by controlling $\vec{\psi}_{\rm c}$.

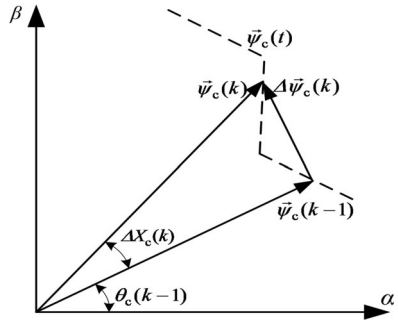

Fig. 2. CW flux linkage space vector.

IV. Schematic Diagram of ISC Control Scheme With Reactive Power Controller

A. CW Flux Linkage Space Vector Increment [19]

Fig. 2 shows the endpoint trajectory of the CW flux linkage space vector $\vec{\psi}_{\rm c}(t)$, approximately expressed as a polygon. Under ideal conditions, the polygonal trajectory will converge to form a circle. The radius of the ideal trajectory is defined by the amplitude of $\vec{\psi}_{\rm c}$. In Fig. 2, $\vec{\psi}_{\rm c}(k)$ and $\vec{\psi}_{\rm c}(k-1)$ are the CW flux linkage space vectors in two adjacent sampling periods, and $\Delta\vec{\psi}_{\rm c}(k)$ is the increment given by

$$\Delta\vec{\psi}_{\rm c}(k) = \vec{\psi}_{\rm c}(k) - \vec{\psi}_{\rm c}(k-1). \quad (18)$$

To express amplitude increment and phase increment of $\vec{\psi}_{\rm c}$ in terms of $k_s(k)$ and $\Delta X_{\rm c}(k)$, respectively, $\vec{\psi}_{\rm c}(k)$ can also be expressed as

$$\vec{\psi}_{\rm c}(k) = e^{j\Delta X_{\rm c}(k)}(1 + K_s(k))\vec{\psi}_{\rm c}(k-1) \quad (19)$$

where the phase increment $\Delta X_{\rm c}(k)$ indicates the sum of the dynamic phase increment $\Delta X_d(k)$ and the static phase increment $\Delta X_{\rm st}(k)$; hence, it can be presented as

$$\Delta X_{\rm c}(k) = \Delta X_{\rm st}(k) + \Delta X_d(k). \quad (20)$$

When the shaft speed is equal to its reference value, then $\Delta X_d = 0$ and $\Delta X_{\rm c} = \Delta X_{\rm st}$. The static phase increment $\Delta X_{\rm st}$

can be expressed as [19]

$$\Delta X_{\rm st} = \omega_{\rm c} T_{\rm pwm} \tag{21}$$

where $T_{\rm pwm}$ is the sampling period, $\omega_{\rm c}$ is CW angular frequency and $\omega_{\rm c} = \pm 2\pi f_{\rm c}$, in which the symbols "+" and "−" represent the supersynchronous and subsynchronous states, respectively, $f_{\rm c}$ is for the shaft speed to decide and the shaft speed $n = \frac{60(f_{\rm p} \pm f_{\rm c})}{p_{\rm p}+p_{\rm c}}$. In the ISC control system for BDFIM, k_s and ΔX_d are the output of flux and torque controller (as shown in Fig. 3), respectively, and will be mentioned in Section IV-C of this chapter.

Considering (19), the increment of $\vec{\psi}_{\rm c}$ in (18) can also be expressed as

$$\Delta\vec{\psi}_{\rm c}(k) = \{e^{j\Delta X_{\rm c}(k)}[1+K_s(k)]-1\}\vec{\psi}_{\rm c}(k-1). \tag{22}$$

By using the following Euler transformation

$$e^{j\Delta X_{\rm c}(k)} = \cos\Delta X_{\rm c}(k) + j\sin\Delta X_{\rm c}(k).$$

$\Delta\vec{\psi}_{\rm c}(k)$ can be rewritten as follows:

$$\Delta\vec{\psi}_{\rm c}(k) = \Delta\psi_{\alpha c}(k) + j\Delta\psi_{\beta c}(k) \tag{23}$$

where $\Delta\psi_{\alpha c}(k)$ and $\Delta\psi_{\beta c}(k)$ are $\alpha\beta$ components of the $\Delta\vec{\psi}_{\rm c}(k)$ and

$$\begin{aligned}\Delta\psi_{\alpha c}(k) = {} & [(1+K_s(k))\cos\Delta X_{\rm c}(k))-1]\psi_{\alpha c}(k-1)\\ & - (1+K_s(k))\sin\Delta X_{\rm c}(k)\psi_{\beta c}(k-1)\\ \Delta\psi_{\beta c}(k) = {} & [(1+K_s(k))\cos\Delta X_{\rm c}(k)-1]\psi_{\beta c}(k-1)\\ & + (1+K_s(k))\sin\Delta X_{\rm c}(k)\psi_{\alpha c}(k-1).\end{aligned} \tag{24}$$

Equation (24) indicates that $\Delta\psi_{\alpha c}(k)$ and $\Delta\psi_{\beta c}(k)$ can be calculated by the variables $K_s(k)$, $\Delta X_{\rm c}(k)$, $\psi_{\alpha c}(k-1)$, and $\psi_{\beta c}(k-1)$.

B. Reactive Power Regulation

Discretizing (17), consequently obtained the reactive power in the *k*th sampling period as follows:

$$\begin{aligned}Q_{\rm p}(k) = {} & -\frac{3}{2}A_1{\rm Im}\Big[L_{\rm hc}L_{\rm hp}\vec{\psi}_{\rm c}^{*}(k)\vec{u}_{\rm p}(k)\\ & + A_2\frac{1}{\omega_{\rm c}}\vec{u}_{\rm p}^{*}(k)e^{-j\frac{\pi}{2}}\vec{u}_{\rm p}(k)\Big].\end{aligned} \tag{25}$$

In similar expression of (19), $\vec{\psi}_{\rm c}^{*}(k)$ in (25) can be represented as

$$\vec{\psi}_{\rm c}^{*}(k) = e^{-j\Delta X_{\rm c}(k)}(1+k_s(k))\vec{\psi}_{\rm c}^{*}(k-1). \tag{26}$$

PW voltage $\vec{u}_{\rm p}(k)$ in (25) also can be expressed as follows:

$$\vec{u}_{\rm p}(k) = e^{j\Delta X_{pc}(k)}\vec{u}_{\rm p}(k-1) \tag{27}$$

where $\Delta X_{pc}(k)$ is the phase increment of $\vec{u}_{\rm p}(k)$. As PW is connected directly to the power grid, its amplitude increment could be seen as zero.

Considering (20), (26), and (27), (25) can be rewritten as follows:

$$\begin{aligned}Q_{\rm p}(k) = {} & -\frac{3}{2}A_1{\rm Im}\Big[L_{\rm hc}L_{\rm hp}e^{j(\Delta X_{pc}(k)-\Delta X_{\rm st}(k)-\Delta X_d(k))}\\ & (1+K_s(k))\vec{\psi}_{\rm c}^{*}(k-1)\vec{u}_{\rm p} - jA_2\frac{1}{\omega_{\rm c}}|\vec{u}_{\rm p}|^2(k-1)\Big].\end{aligned} \tag{28}$$

If the dynamic phase increment ΔX_d in (28) is small enough, then $\sin\Delta X_d \approx \Delta X_d$, by using this approximate expression, $Q_{\rm p}(k)$ can be simplified as shown in (48) in Appendix III and expressed as

$$\begin{aligned}Q_{\rm p}(k) = {} & C(\sin\Delta X_d(k-1) + \Delta X_d(k)\cos\Delta X_d(k-1)\\ & + K_s(k)\sin\Delta X_d(k-1)) + \frac{3}{2}A_1A_2\frac{1}{\omega_{\rm c}}|\vec{u}_{\rm p}|^2(k-1)\end{aligned} \tag{29}$$

where

$$C = \frac{3}{2}A_1\left[L_{\rm hc}L_{\rm hp}\left|\vec{\psi}_{\rm c}(k-1)\right||\vec{u}_{\rm p}(k-1)|\right].$$

Similarly, with consideration to (17), $Q_{\rm p}(k-1)$ can be expressed as

$$\begin{aligned}Q_{\rm p}(k-1) = {} & -\frac{3}{2}A_1{\rm Im}\Big[L_{\rm hc}L_{\rm hp}\vec{\psi}_{\rm c}^{*}(k-1)\vec{u}_{\rm p}(k-1)\\ & + A_2\frac{1}{\omega_{\rm c}}\vec{u}_{\rm p}^{*}(k-1)e^{-j\frac{\pi}{2}}\vec{u}_{\rm p}(k-1)\Big]\\ = {} & C\sin\Delta X_d(k-1) + \frac{3}{2}A_1A_2\frac{1}{\omega_{\rm c}}|\vec{u}_{\rm p}|^2(k-1).\end{aligned} \tag{30}$$

Considering (29) and (30), $Q_{\rm p}(k)$ can finally be expressed as

$$\begin{aligned}Q_{\rm p}(k) = {} & Q_{\rm p}(k-1) + \Delta Q_{\rm p}(k) = Q_{\rm p}(k-1)\\ & + K_3(k-1)\Delta X_d(k) + k_4(k-1)k_s(k)\end{aligned} \tag{31}$$

where $\Delta Q_{\rm p}(k)$ is the reactive power increment in the *k*th sampling period and

$$\begin{aligned}&\Delta Q_{\rm p}(k) = K_3(k-1)\Delta X_d(k) + K_4(k-1)K_s(k)\\ &K_3(k-1) = C\cos\Delta X_d(k-1)\\ &= \frac{3}{2}A_1[L_{\rm hc}L_{\rm hp}\left|\vec{\psi}_{\rm c}(k-1)\right||\vec{u}_{\rm p}(k-1)|]\cos\Delta X_d(k-1)\\ &K_4(k-1) = C\sin\Delta X_d(k-1)\\ &= \frac{3}{2}A_1[L_{\rm hc}L_{\rm hp}\left|\vec{\psi}_{\rm c}(k-1)\right||\vec{u}_{\rm p}(k-1)|]\sin\Delta X_d(k-1).\end{aligned} \tag{32}$$

C. Proposed ISC Scheme With Reactive Power Control

It has been derived that the electromagnetic torque in the *k*th sampling period can be expressed as [19]

$$\begin{aligned}T_e(k) = {} & T_e(k-1) + \Delta T_e(k) = T_e(k-1)\\ & + K_1(k-1)\Delta X_d(k) + K_2(k-1)K_s(k)\end{aligned} \tag{33}$$

where $\Delta T_e(k)$ is the torque increment and detailed expressions for $K_1(k-1)$ and $K_2(k-1)$ can be expressed as

$$\begin{aligned}\Delta T_e(k) = {} & K_1(k-1)\Delta X_d(k) + K_2(k-1)K_s(k)\\ K_1(k-1) = {} & T_{ecr}\cos\theta_{cr}(k-1) - T_{epc}\cos\theta_{pc}(k-1)\\ K_2(k-1) = {} & T_{ecr}\sin\theta_{cr}(k-1) + T_{epc}\sin\theta_{pc}(k-1)\end{aligned} \tag{34}$$

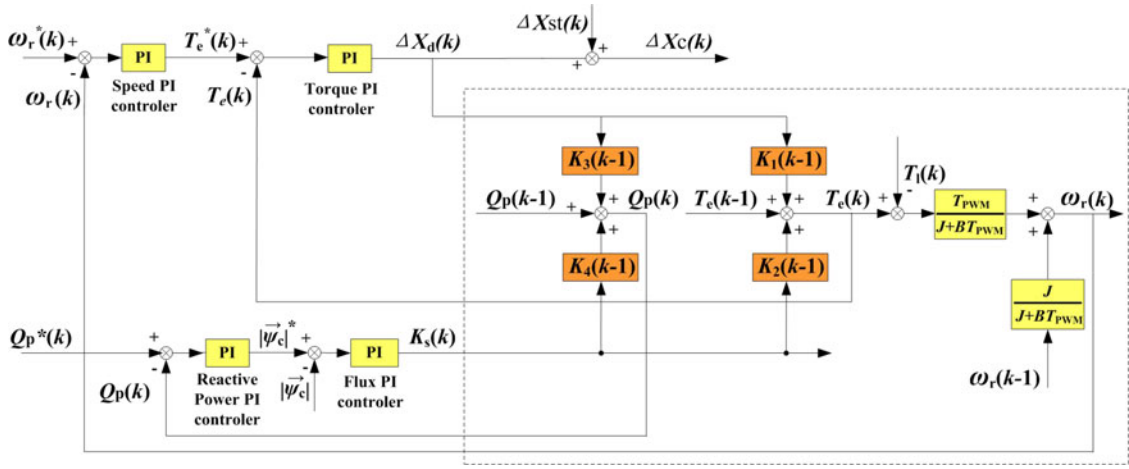

Fig. 3. Schematic diagram for BDFIM ISC control system.

where detailed expressions for T_{ecr}, T_{epc} and θ_{cr}, θ_{pc} can be found in [19].

Equations (31)–(34) show the relationship between the increment of the torque, the increment of the reactive power and the dynamic phase increment ΔX_d, and the amplitude increment k_s.

The discrete mechanical differential equation can be found in [19]

$$\omega_{\rm r}(k) = \frac{T_{\rm pwm}}{J + BT_{\rm pwm}}\left(T_e(k) - T_{\rm l}(k)\right) + \frac{J}{J + BT_{\rm pwm}}\omega_{\rm r}(k-1) \tag{35}$$

where $T_{\rm l}$ is regarded as the load torque, J is the moment of inertia, and B is the friction coefficient. From (35), it is easily apparent that the mechanical angular speed $\omega_{\rm r}$ can be regulated by controlling $T_{\rm e}$.

Equations (31), (33), and (35) constitute the equations for BDFIM ISC control. Based on this set of equations, a structure diagram was obtained as shown in the dot outlined in Fig. 3. Fig. 3 is the schematic diagram for the BDFIM ISC control system, in which four controllers are used to regulate speed, reactive power, flux amplitude, and torque. As shown in Fig. 3, the speed and reactive power are outer loops, and the torque and flux amplitude are inner loops. The output of the torque PI controller is ΔX_d, and ΔX_d plus $\Delta X_{\rm st}$ is $\Delta X_{\rm c}$. The regulatory process of torque or speed is explained as follows: it is assumed that the BDFIM is running steadily at a mechanical angular speed of $\omega_{\rm r} = \omega_{\rm r}^*$, then $\Delta X_d = 0$ and $\Delta X_{\rm c} = \Delta X_{\rm st}$, where $\Delta X_{\rm st}$ is determined by the shaft speed. If the torque or speed varies, ΔX_d is changed through the regulation of the torque or speed PI controller and $\Delta X_{\rm st}$ varies with shaft speed. As a result,$\Delta X_{\rm c}$, as seen in Fig. 3, also changes and the variation in the $\Delta X_{\rm c}$ results in changes in $\omega_{\rm r}$. The regulatory process continues until a new steady state is achieved.

As shown in Fig. 3, reactive power control is achieved by controlling $\left|\vec{\psi}_{\rm c}\right|$. The reactive power controller in Fig. 3 receives an error signal with respect to the output $\left|\vec{\psi}_{\rm c}\right|^*$, and the flux PI controller is used to regulate the dynamic performance of reactive power. As indicated in (4), $|\vec{u}_{\rm c}|$ changes with $\left|\vec{\psi}_{\rm c}\right|$, so, to control reactive power by adjusting $\left|\vec{\psi}_{\rm c}\right|$ is similar to by adjusting $|\vec{u}_{\rm c}|$ in nature [22].

Similar to an electrically excited synchronous generator, there is a cross coupling between $Q_{\rm p}$ and T_e. That is to say, change in ΔX_d affects $Q_{\rm p}$ and similarly, the change in k_s would also affect T_e. However, the controllers in Fig. 3 would timely adjust the output, eliminating errors between the reference and feedback values, and the system will eventually operate steadily near its reference value. In experiments, the response of the reactive power loop is regulated to go faster, making the system more readily stable. In addition, T_e^*, ΔX_d, and k_s have a saturated value to provide current-limit. Compared to the controller schematic diagram previously proposed [19], an outer control loop to regulate $Q_{\rm p}$ is added. Based on the control loop illustrated above, a block diagram of the ISC system with reactive power controller for the BDFIM is drawn in Fig. 4.

In Fig. 4, $\Delta\vec{\psi}_{\alpha c}$ and $\Delta\vec{\psi}_{\beta c}$ can be calculated by $\Delta X_{\rm c}$ and k_s as shown in (24), which are required to determine the CW reference voltages $u_{\alpha c}$ and $u_{\beta c}$ as shown in (36) [19]. $u_{\alpha c}$ and $u_{\beta c}$ are the inputs of the pulse width modulation (PWM) generator, which produces switching signals for the converter driving the CW of the BDFIM.

$$\begin{aligned} U_{\alpha c} &= \frac{\Delta\psi_{\alpha c}}{T_{\rm pwm}} + R_{\rm c} i_{\alpha c} \\ U_{\beta c} &= \frac{\Delta\psi_{\beta c}}{T_{\rm pwm}} + R_{\rm c} i_{\beta c}. \end{aligned} \tag{36}$$

D. Reactive Power, Flux Linkage, and Torque Estimator

As shown in Fig. 4, accurately estimating the reactive power, electromagnetic torque, and CW flux in the ISC system is of great importance.

Considering (38) (see Appendix I), using the $\alpha\beta$ components of PW currents and voltages, the PW reactive power can also be

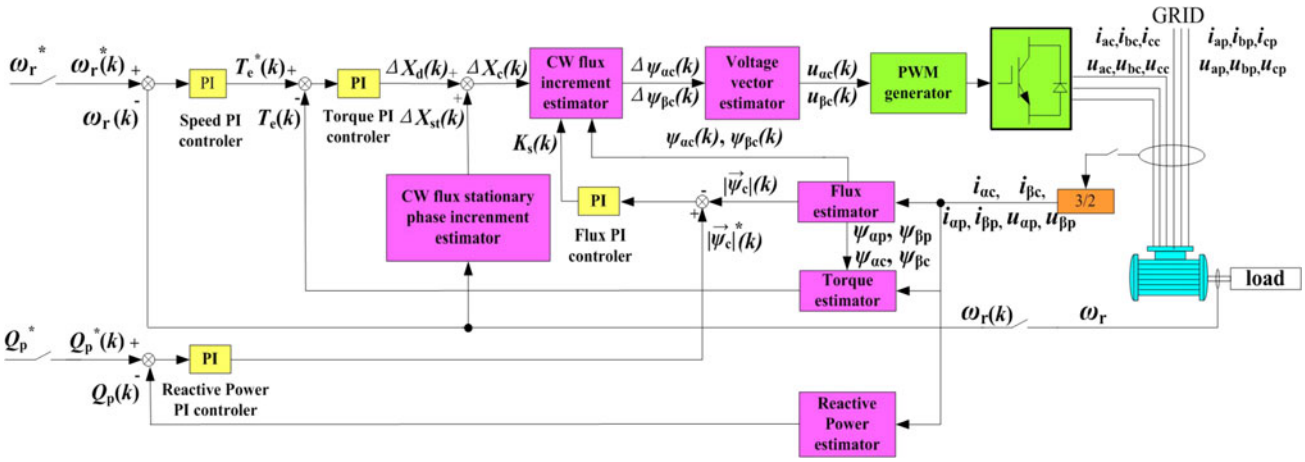

Fig. 4. Block diagram of the proposed ISC control system with reactive power controller.

Fig. 5. Test rig.

TABLE 1
PROTOTYPE PARAMETERS

Parameter	Value	Parameter	Value
Frame size	D160	CW rated current	3.6 A
PW pole-pairs	3	Rated torque	32 N · m
CW pole-pairs	1	L_{hc}	4 mH
RW pole-pairs	4	L_{r}	0.048 mH
Natural speed	750 r/min	R_{p}	3.2 Ω
PW rated power	3 kW at 50 Hz	R_{c}	5.32 Ω
CW rated power	1.5 kW at 50 Hz	R_{r}	0.173 mΩ
PW rated voltage	380 V at 50 Hz	L_{p}	292 mH
CW rated voltage	380 V at 50 Hz	L_{hp}	2.16 mH
PW rated current	5.8 A	L_{c}	642 mH

written as

$$Q_{\mathrm{p}} = \frac{3}{2}\mathrm{Im}(\vec{u}_{\mathrm{p}}^{(1)}\vec{i}_{\mathrm{p}}^{*(1)}) = \frac{3}{2}(u_{\beta\mathrm{p}}i_{\alpha\mathrm{p}} - u_{\alpha\mathrm{p}}i_{\beta\mathrm{p}}). \tag{37}$$

The estimation of $\psi_{\alpha p}$, $\psi_{\beta p}$, $\psi_{\alpha c}$, $\psi_{\beta c}$, and T_e can also be achieved by using currents and voltages of PW and CW own $\alpha\beta$ values as presented in [19].

As mentioned previously, PW reactive power, flux, and electromagnetic torque are estimated in PW and CW own $\alpha\beta$ values. That is to say, although Figs. 3 and 4 are derived from the CW static reference frame, the PW variables need not be transformed into the CW static reference frame in the actual system, so the rotating coordinate transformations may be avoided.

V. EXPERIMENTAL RESULTS

A. Experimental Setup

An experimental setup was used to evaluate the performance of the proposed reactive power control scheme (see Fig. 5). This test rig is the same as used in [19] and presented again in this paper for convenience of reference. The physical data and parameters of the prototype BDFIM are provided in Table I. The pole pair numbers of the PW and CW are 3 and 1, respectively. The rotor of the prototype is a nested cage design (see Figs. 6 and 7). It has four nests with five loops per nest. A direct current (dc) generator acted as a load machine, and a resistance box was used as the load for the dc generator. Speed signals were obtained from an incremental encoder (OMRON E6C2-CWZ6C). A back-to-back two-level converter supplied the CW of the BDFIM, and the PW is directly connected to the

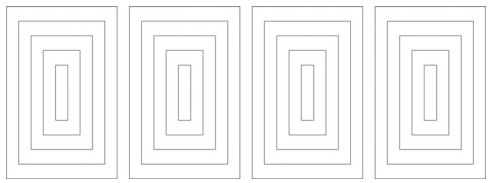

Fig. 6. Prototype rotor winding structure.

Fig. 7. Prototype rotor.

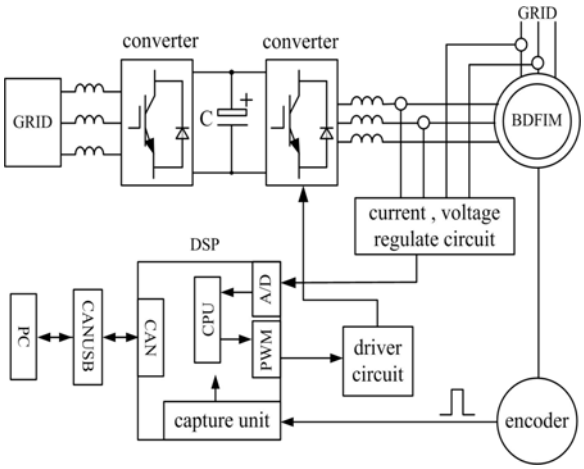

Fig. 8. Schematic diagram of the converter.

grid (380 V, 50 Hz). Fig. 8 shows the schematic diagram of the converter. The control algorithm was implemented on a digital signal processor (DSP, TMS320LF2407A). The PW voltage and the currents of two stator windings were measured with the LEM LV 25-p and LEM LA 58-p modules, respectively. A USB–CAN interface card (Guangzhou Zhiyuan Electronic Co. Ltd, China) was used to provide the connection between the communication interfaces (i.e., CAN of the DSP and USB of the PC). Thus, the bidirectional data transfer between the DSP and PC was properly established. The sampling time of the control loop was 0.5 ms. All PI parameters for PW reactive power, speed, torque, and flux linkage controllers were tuned throughout the experiments. The saturated value of ΔX_d and k_s are 0.006rad and 0.03, respectively.

When started, the converter is controlled to short the CW so that the BDFIM is in cascade mode. Upon approaching natural speed, the controller switches to the synchronous mode.

B. Step Reactive Power Response

Fig. 9 shows the response of the machine to a step change in the reactive power while the reference speed is set at 855r/min, and an electromagnetic torque $T_{\rm e}$ of 14 N · m is applied to the BDFIM. As shown in Fig. 9(a), the PW reactive power is stably controlled from 500 to −250 var with a fall time of 600 ms and an overshoot of 0%. During the dynamic process, the speed is well regulated at its reference value of 855 r/min, as given in Fig. 9(b). Torque is kept at approximately 14 N · m, as shown in Fig. 9(c). CW flux amplitude is increased to 1.16 Wb according to the decrease of the reactive power absorbed from grid as shown in Fig. 9(d). CW and PW currents increase to compensate for the change in the reactive power, as shown in Fig. 9(e)and (f). Fig. 9 shows that the proposed controller can be used to control the reactive power flow of the PW from absorbing reactive power to exporting.

C. Step Torque Response

A step torque changes first from 0 to 14 N · m and then down to 0 N · m is applied to the BDFIM to test the stability of the system shown in Fig. 10(a). Fig. 10(b) shows that there is a maximum oscillating amplitude of about 77% in the reactive power, but it quickly returns to the reference value. As shown in Fig. 10(c), the speed is well regulated at its reference value of 840 r/min, with a maximum oscillating amplitude of 11%. Fig. 10(d) and (e) shows that, since the machine load varies, reactive power changes, which makes CW current and flux amplitude change accordingly to compensate for the disturbance and keep the reactive power constant. As shown in Fig. 10 (f), the increase in the torque causes change in the PW input power, the PW currents increase accordingly, vice versa. Fig. 10(g) and (h) is the expanded waveform of the CW and PW loading currents.

D. Step Speed Response

Fig. 11 illustrates the experimental results from a change in demand speed. The BDFIM speed is controlled from 615 to 885r/min with an overshoot of 3.9% as shown in Fig. 11(a). Fig. 11(b) shows that the torque is increased because the armature voltage of the dc generator rises while its load is unchanged. The reference PW reactive power is set at 450var as shown in Fig. 11(c). The reactive power response shows a maximum oscillating amplitude of about 26%, but it quickly returns to the reference value. Again, as shown in Fig. 11(d) and (e), since the machine speed and torque vary, the reactive power changes, which, accordingly makes the CW current and flux amplitude change to compensate for the disturbance and keep the reactive power constant. As shown in Fig. 11(f), due to an increase in speed and the torque, the PW input power increases, so the PW currents increase.

E. Ramp Torque Response

Figs. 10 and 11 show that when the reference reactive power $Q_{\rm p}^*$ remains unchanged, the reactive power $Q_{\rm p}$ will be effected by a change in either the torque or the speed, namely there is a cross coupling between the reactive power and the speed (or torque). However, Figs. 10 and 11 are step response, and such fast transients are not imperative for some applications such as fans or pumps, etc. When ramp input is employed, the influence between the speed (or torque) and the reactive power can be obviously reduced. Fig. 12 is the torque ramp response from 14 to 0 N · m, with a fall time of approximately 2.3 s and where the other conditions are the same as in Fig. 10. Due to the load resistance of the dc generator cannot be adjusted smoothly, the torque decline curve is not linear as shown in Fig. 12(a). In comparison with the torque step response, the maximum oscillating amplitude of the reactive power is reduced from 77% to 16.7%, and the oscillating amplitude of the speed is reduced from 11% to 2.7%.

The experiment results show that the coupling effect is strongest in the step response. In the ramp response, the smaller the slope is, the smaller the impact of coupling is.

VI. Conclusion

This paper adds a reactive power control to the ISC strategy for BDFIM. As a result, both speed and the reactive power can

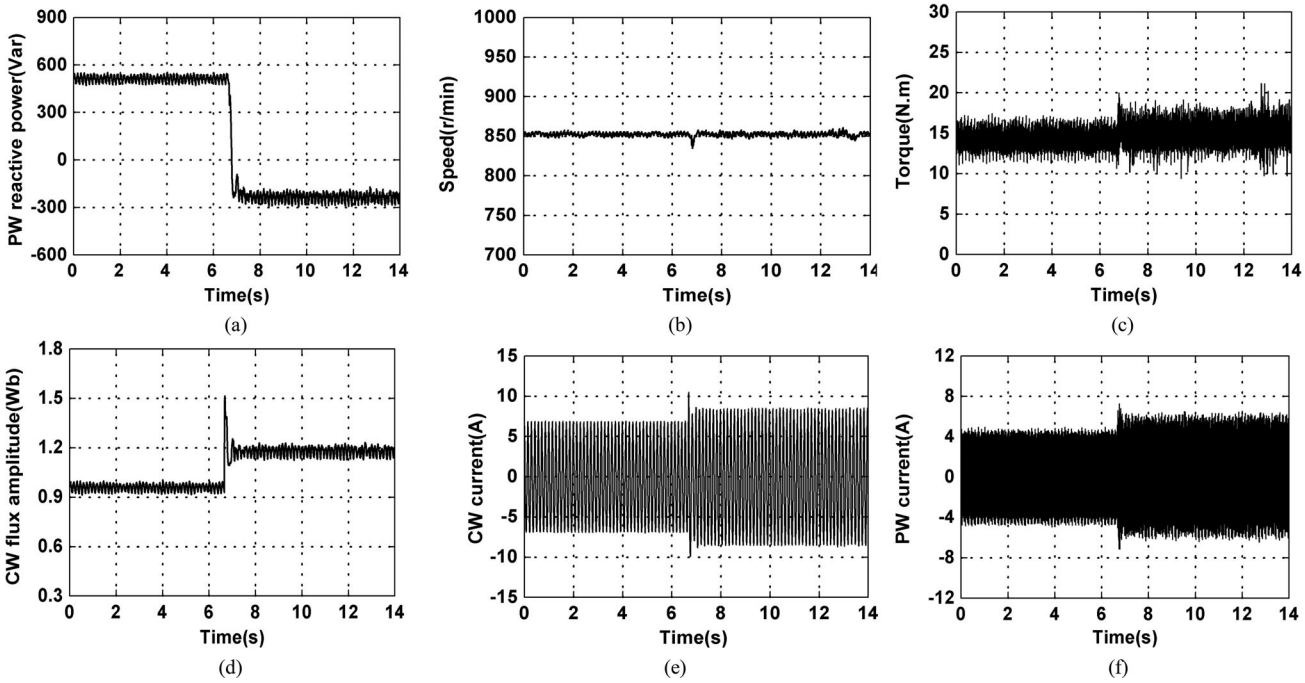

Fig. 9. Experimental results for a reactive power change. The given speed is kept constant at 855 r/min. (a) PW reactive power. (b) Shaft speed. (c) Torque.(d) CW flux amplitude. (e) CW currents. (f) PW currents.

be controlled. These control features are achieved in a static reference frame, and rotating coordinate transformations and flux linkage orientation are unnecessary, so the ISC is simpler to implement. The experimental results show stable operation under various controlling commands. All the characteristics show the potential of employing ISC in a practical industry environment.

APPENDIX I
PW REACTIVE POWER IN CW STATIC REFERENCE FRAME

In PW static reference frame, the PW reactive power can be written as

$$Q_{\rm p} = \frac{3}{2}{\rm Im}(\vec{u}_{\rm p}^{(1)}\vec{i}_{\rm p}^{*(1)}). \tag{38}$$

Considering the following transformations between PW and CW static reference frames

$$\begin{aligned}\vec{u}_{\rm p}^{(1)} &= e^{-k}\vec{u}_{\rm p}^{*}\\ \vec{i}_{\rm p}^{*(1)} &= e^{k}\vec{i}_{\rm p}.\end{aligned} \tag{39}$$

Therefore, PW reactive power referred to CW static reference frame can be expressed as (7), which is as follows

$$Q_{\rm p} = \frac{3}{2}\,{\rm Im}\left(\vec{i}_{\rm p}^{*}\vec{u}_{\rm p}\right)$$

where k is defined as the angular speed [19], $k = -j\left[(\omega_{a1}+\omega_{a2}) - (p_{\rm p}+p_{\rm c})\omega_{\rm r}\right]t$, where ω_{a1} and ω_{a2} are angular frequencies of two PW and CW reference frames, respectively, when PW and CW reference frames are static, $\omega_{a1} = \omega_{a2} = 0$.

APPENDIX II
DERIVATION OF EQUATION (16)

For simplicity, the PW resistance voltage drop is ignored, (4) can be rewritten as

$$\vec{u}_{\rm p} \approx \frac{d\vec{\psi}_{\rm p}}{dt} - j(p_{\rm p}+p_{\rm c})\omega_{\rm r}\vec{\psi}_{\rm p}. \tag{40}$$

$\vec{\psi}_{\rm p}$ in (40) can be expressed as

$$\vec{\psi}_{\rm p} = \left|\vec{\psi}_{\rm p}\right| e^{j\omega_{\rm p}t} \tag{41}$$

where $\omega_{\rm p}$ is PW angular frequency, $\left|\vec{\psi}_{\rm p}\right|$ is the magnitude of PW flux.

Consider BDFIM mechanical angular speed

$$\omega_{\rm r} = \frac{\omega_{\rm p}+\omega_{\rm c}}{p_{\rm p}+p_{\rm c}}. \tag{42}$$

Substituting (41) and (42) into (40), $\vec{\psi}_{\rm p}$ can be expressed in the CW static reference frame as (16), which is as follows:

$$\vec{\psi}_{\rm p} = \frac{1}{\omega_{\rm c}}\vec{u}_{\rm p}e^{j\frac{\pi}{2}}.$$

APPENDIX III
SIMPLIFICATION OF THE REACTIVE POWER

In the CW static reference frame, the angular frequency of PW and CW are all $\omega_{\rm c}$, so in a sample period

$$\Delta X_{\rm pc}(k) = \Delta X_{\rm st}(k)$$

and

$$\vec{\psi}_{\rm c}^{*}(k-1)\vec{u}_{\rm p}(k-1) =$$

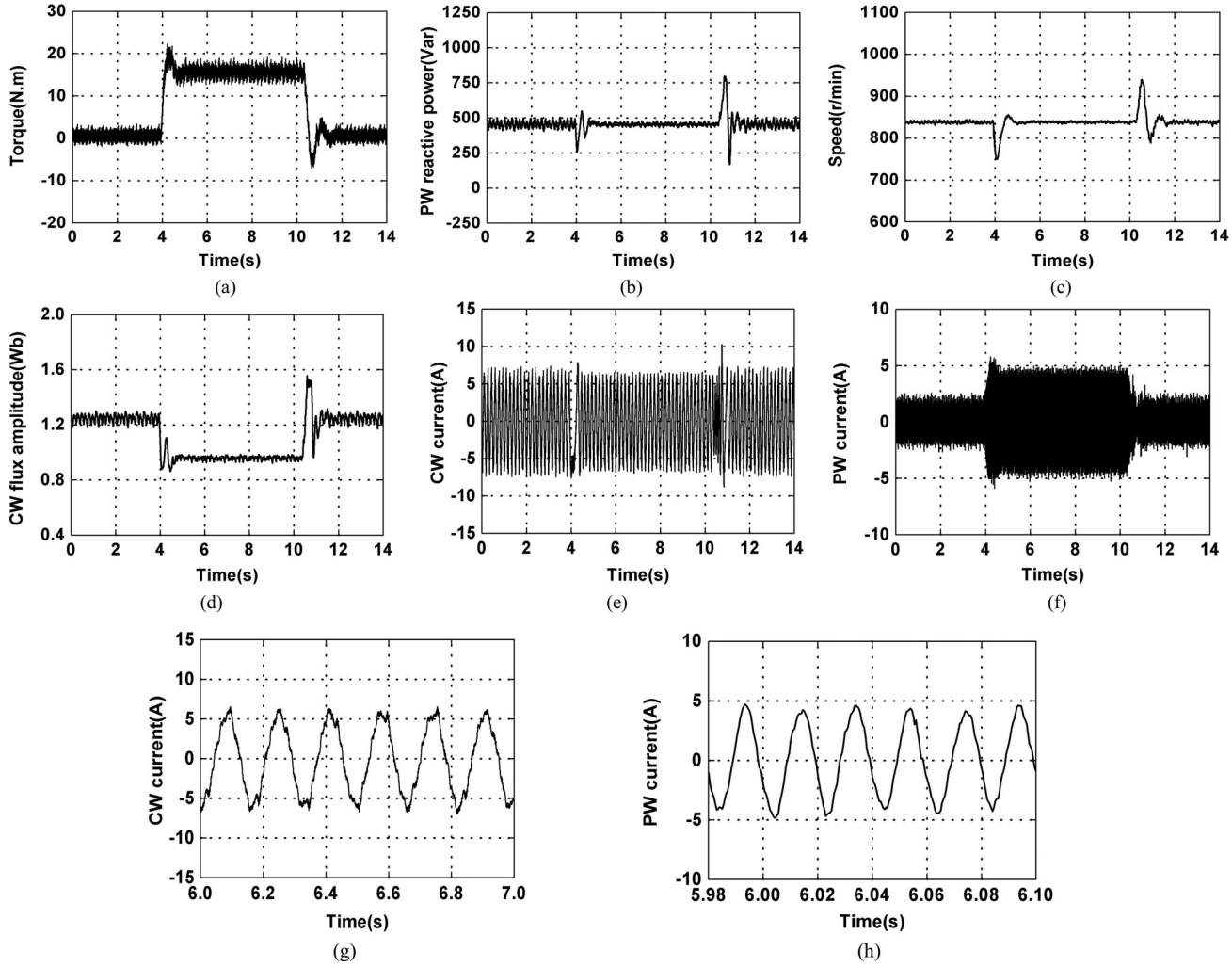

Fig. 10. Experimental results for a torque step change. The given speed is kept constant at 840 r/min. (a) Torque. (b) PW reactive power. (c) Shaft speed. (d) CW flux amplitude. (e) CW currents. (f) PW currents. (g)Expanded waveforms of the CW loading currents. (h) Expanded waveforms of the PW loading currents.

$$\begin{aligned}&\left|\vec{\psi}_{\rm c}(k-1)\right| |\vec{u}_{\rm p}(k-1)|\, e^{j(\Delta X_{pc}(k-1)-\Delta X_{\rm c}(k-1))}\\ &\quad=\left|\vec{\psi}_{\rm c}(k-1)\right| |\vec{u}_{\rm p}(k-1)|\, e^{j(\Delta X_{st}(k-1)-\Delta X_{\rm c}(k-1))}\\ &\quad=\left|\vec{\psi}_{\rm c}(k-1)\right| |\vec{u}_{\rm p}(k-1)|\, e^{-j(\Delta X_d(k-1))}\end{aligned}\tag{43}$$

where $\Delta X_{\rm st}(k-1)$ and $\Delta X_d(k-1)$ are the static phase increment and the dynamic phase increment in the $k{-}1^{\rm th}$ sampling period.

By substituting (43) into (28), $Q_{\rm p}(k)$ can be simplified as

$$\begin{aligned}&Q_{\rm p}(k)=\\ &-\frac{3}{2}A_1{\rm Im}\left[L_{\rm hc}L_{\rm hp}(1+K_s(k))\left|\vec{\psi}_{\rm c}(k-1)\right||\vec{u}_{\rm p}(k-1)|\right.\\ &\left.e^{j(-\Delta X_d(k-1)+\Delta X_{pc}(k)-\Delta X_{\rm c}(k))}-jA_2\frac{1}{\omega_{\rm c}}|\vec{u}_{\rm p}|^2(k-1)\right]\\ &=\frac{3}{2}A_i\left[L_{\rm hc}L_{\rm hp}(1+K_s(k))\left|\vec{\psi}_{\rm c}(k-1)\right||\vec{u}_{\rm p}(k-1)|\right.\\ &\left.\sin(\Delta X_d(k-1)+\Delta X_d(k))+A_2\frac{1}{\omega_{\rm c}}|\vec{u}_{\rm p}|^2(k-1)\right].\end{aligned}\tag{44}$$

Since the ΔX_d in (44) is small enough, then approximations can be found in (45)

$$\begin{aligned}&\sin(\Delta X_d(k-1)+\Delta X_d(k))=\sin\Delta X_d(k-1)\cos\Delta X_d(k)\\ &+\cos\Delta X_d(k-1)+\sin\Delta X_d(k)\\ &\approx\sin\Delta X_d(k-1)\Delta X_d(k)+\cos\Delta X_d(k-1).\end{aligned}\tag{45}$$

Eq. (44) can be further simplified by substituting (45) into (44) as follows:

$$\begin{aligned}Q_{\rm p}(k)=\ &\frac{3}{2}A_1\left[L_{\rm hc}L_{\rm hp}\left|\vec{\psi}_{\rm c}(k-1)\right||\vec{u}_{\rm p}(k-1)|(1+k_s(k))\right.\\ &(\sin\Delta X_d(k-1)+\Delta X_d\cos\Delta X_d(k-1))\\ &\left.+A_2\frac{1}{\vec{\omega}_{\rm c}}|\vec{u}_{\rm p}|^2(k-1)\right].\end{aligned}\tag{46}$$

Since both $\Delta X_d(k)$ and $K_s(k)$ are very small, the product of $K_s(k)$ and $\Delta X_d(k)$ can be omitted, then approximations can

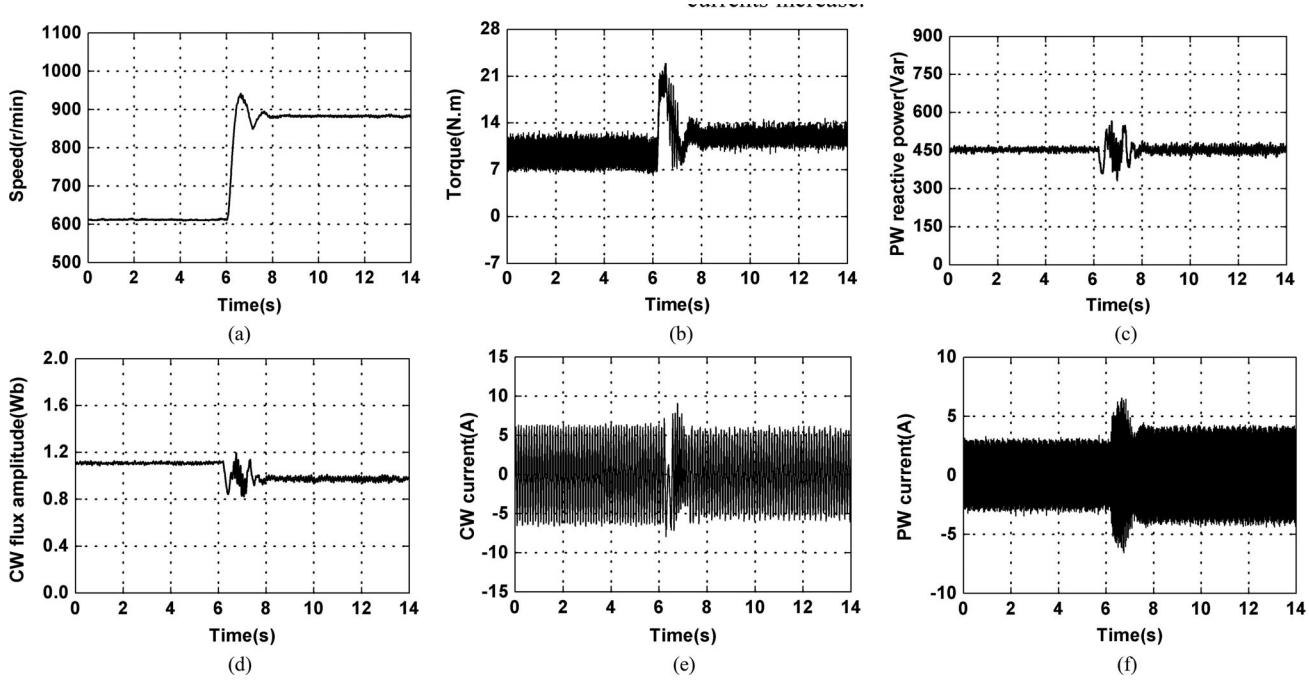

Fig. 11. Experimental results for a speed step change. The given reactive power is kept constant at 450 var. (a) Shaft speed. (b) Torque. (c) PW reactive power. (d) CW flux amplitude. (e) CW currents. (f) PW currents.

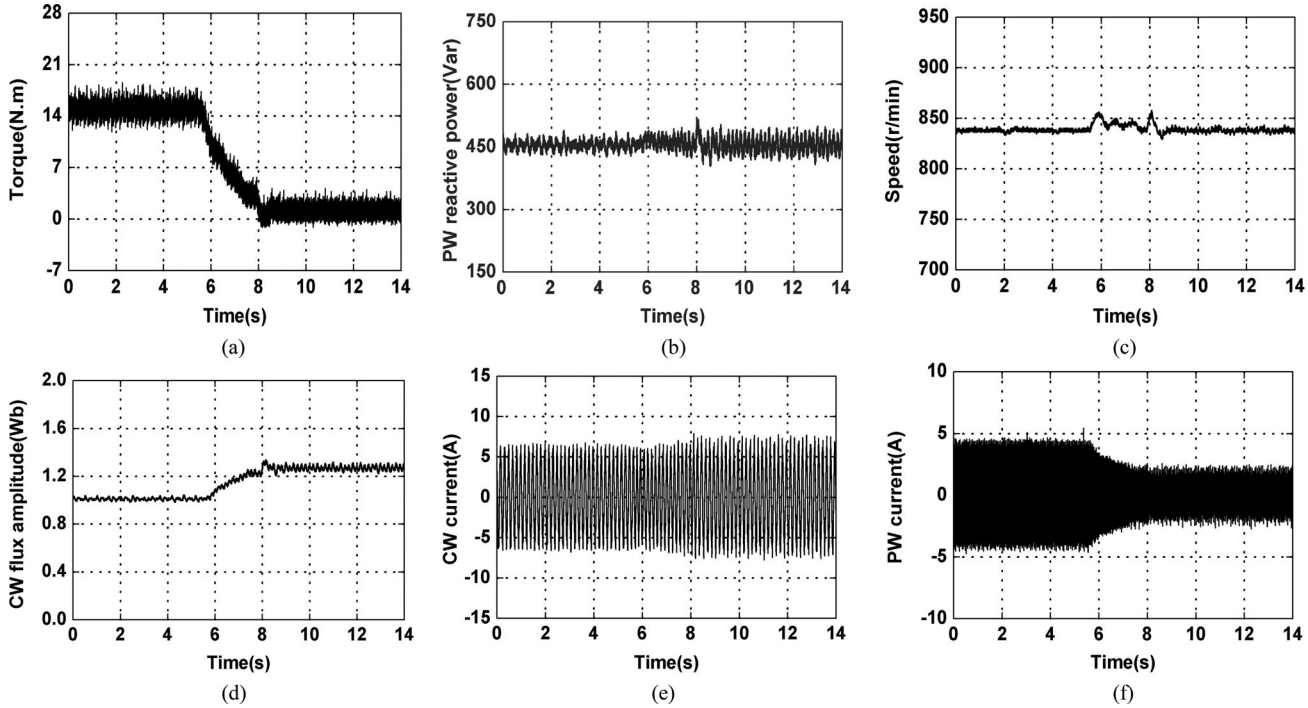

Fig. 12. Experimental results for a torque ramp change. The given speed is kept constant at 840 r/min. (a) Torque. (b) PW reactive power. (c) Shaft speed. (d) CW flux amplitude. (e) CW currents. (f) PW currents.

be found in (47)

$$\begin{aligned}&(1+k_s(k))\left(\sin\Delta X_d(k-1)+\Delta X_d(k)\cos\Delta X_d(k-1)\right)\\&=\sin\Delta X_d(k-1)+\Delta X_d(k)\cos\Delta X_d(k-1)\\&+k_s(k)\sin\Delta X_d(k-1)\\&+k_s(k)\Delta X_d(k)\cos\Delta X_d(k-1)\\&\approx\sin\Delta X_d(k-1)+\Delta X_d(k)\cos\Delta X_d(k-1)\\&+k_s(k)\sin\Delta X_d(k-1).\end{aligned}\tag{47}$$

Substituting (47) into (46), $Q_{\mathrm{p}}(k)$ can finally be simplified as

$$\begin{aligned} Q_{\mathrm{p}}(k) &= \frac{3}{2}A_1\left[L_{\mathrm{hc}}L_{\mathrm{hp}}\left|\vec{\psi}_{\mathrm{c}}(k-1)\right|\left|\vec{u}_{\mathrm{p}}(k-1)\right|\right. \\ &(\sin\Delta X_d(k-1)+\Delta X_d(k)\cos\Delta X_d(k-1) \\ &\left.+K_s(k)\sin\Delta X_d(k-1))+A_2\frac{1}{\omega_{\mathrm{c}}}\left|\vec{u}_{\mathrm{p}}\right|^2(k-1)\right] \\ &= C(\sin\Delta X_d(k-1)+\Delta X_d(k)\cos\Delta X_d(k-1) \\ &+K_s(k)\sin\Delta X_d(k-1))+\frac{3}{2}A_1A_2\frac{1}{\omega_{\mathrm{c}}}\left|\vec{u}_{\mathrm{p}}\right|^2(k-1) \quad (48) \end{aligned}$$

where

$$C=\frac{3}{2}A_1\left[L_{\mathrm{hc}}L_{\mathrm{hp}}\left|\vec{\psi}_{\mathrm{c}}(k-1)\right|\left|\vec{u}_{\mathrm{p}}(k-1)\right|\right].$$

REFERENCES

[1] H. Li and Z. Chen, "Overview of different wind generator systems and their comparisons," *IET Renewable Power Gener.*, vol. 2, no. 2, pp. 123–138, 2008.

[2] L. Xu, B. Guan, H. Liu, and L.Gao "Design and control of a high-efficiency doubly-fed brushless machine for wind power generator application," in *Proc. IEEE Energy Convers. Congr. Expo.*, 2010, pp. 2409–2416.

[3] R. A. McMahon, E. Abdi, and S. Shao, "Design and testing of a 250 kW medium-speed brushless DFIG," in *Proc. 6th IET Int. Conf. Power Electron., Mach. Drives*, 2012, pp. 207–212.

[4] T. Long, S. Shao, P. Malliband, E. Abdi, and R. McMahon, "Crowbarless fault ride through of the brushless doubly fed induction generator in a wind turbine under symmetrical voltage dips," *IEEE Trans. Ind. Electron.*, vol. 60, no. 7, pp. 2833–2841, Jul. 2013.

[5] A. K. Wallace and R. Spee, "Dynamic modeling of brushless doubly-fed machine," in *Proc. IEEE IAS Annu. Meet.*, 1989, pp. 329–334.

[6] R. LI, A. K. Wallace, and R. Spee, "Two-axes model development of cage-rotor brushless doubly-fed machines," *IEEE Trans. Energy Convers.*, vol. 6, no. 3, pp. 444–452, Sep. 1991.

[7] M. S Boger and A. K Wallace, "General pole number model of the brushless doubly-fed machine," *IEEE Trans. Ind. Appl.*, vol. 31, no. 5, pp. 1022–1028, Sep. 1995.

[8] J. Poza, E. Oyarbide, D. Roye, and M. Rodriguez, "Unified reference frame dq model of the brushless doubly fed machine," in *Proc. Inst. Elect. Eng, Elect. Power Appl.*, vol. 153, no. 5, pp. 726–734, Sep. 2006.

[9] S. Shao, A. Ehsan, and R. McMahon, "Vector control of the brushless doubly-fed machine for wind power generation," in *Proc. ICSET*, Nov. 2008, pp. 322–327.

[10] S. Shao, A. Ehsan, B. Farhad, and M. Richard, "Stator-flux -oriented vector control for brushless doubly fed induction generator," *IEEE Trans. Ind. Electron.*, vol. 56, no. 10, pp. 4220–4228, Oct. 2009.

[11] J. Poza, E. Oyarbide, and D. Roye, "New vector control algorithm for brushless doubly–fed machines," in *Proc. IEEE 28th Annu. Ind. Electron. Soc. Conf.*, Nov. 2002, vol. 2, pp. 1138–1143.

[12] J. Poza, E. Oyarbide, I. Sarasola, I. Sarasola, and M. Rodriguez,, "Vector control design and experimental evaluation for the brushless doubly fed machine," *IET Electr. Power Appl.*, vol. 3, no. 4, pp. 247–256, Jul. 2009.

[13] S. Tohidi, H. Oraee, S. Shao, and P. Tavner, "Analysis and enhancement of low-voltage ride-through capability of brushless doubly fed induction generator," *IEEE Trans. Ind. Electron.*, vol. 60, no. 3, pp. 1146–1155, Mar. 2013.

[14] I. Takahashi and Y. Ohmori, "High performance direct torque control of an induction motor," *IEEE Trans. Ind. Appl.*, vol. 25, no. 2, pp. 257–264, Mar./Apr. 1989.

[15] I. Sarasola, J. Poza, and M. Rodriguez, "Direct torque control for brushless doubly-fed induction machines," in *Proc. IEEE Int. Electric Mach. Drive. Conf.*, 2007, pp. 1496–1501.

[16] I. Sarasola, J. Poza, M. A. Rodriguez, and G. Abad, "Direct torque control design and experimental evaluation for the brushless doubly fed machine," *Energy Convers. Manag.*, vol. 52, no. 2, pp. 1226–1234, Feb. 2011.

[17] C. Hamza and J. Milutin, "Toward a generic torque and reactive power controller for doubly fed machines," *IEEE Trans. Power Electron.*, vol. 27, no. 1, pp. 113–121, Jan. 2012.

[18] A. Zhang, W. Jia, Z. Zhou, and X. Wang, "A study on indirect stator-quantities control strategy for brushless doubly-fed induction machine," in *Proc. Int. Conf. Electr. Mach. Syst.*, 2011, pp. 1–6.

[19] A. Zhang, X. Wang, W. Jia, and Y. Ma, "Indirect stator-quantities control for the brushless doubly fed induction machine," *IEEE Trans. Power Electron.*, vol. 29, no. 3, pp. 1392–1401, Mar. 2014.

[20] J. Tian, C. Su and Z. Chen, "Reactive power capability of the wind turbine with doubly fed induction generator," in *Proc. 39th Annu. IEEE Ind. Electron. Soc. Conf.*, 2013, pp. 5312–5317.

[21] I. V. Lindell, "Heaviside operational rules applicable to electromagnetic problems," *PIER.*, vol. 26, pp. 293–331, 2000.

[22] R. A. McMahon, P. C. Roberts, X. Wang, and P. J. Tavner, "Performance of BDFM as generator and motor, "*IEE Proc.-Electr. Power Appl.*, vol. 153, no. 2, pp. 289–299, Mar. 2006.

Rongli Zhao received the M.Sc. degree from the Taiyuan University of Technology, Taiyuan, China, in 2002. She is currently working toward the Ph.D. degree in the field of machine control in the same university.

She is currently a Lecturer in the Taiyuan University of Technology.

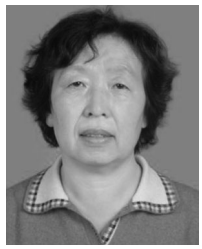

Ailing Zhang received the M.Sc. degree from the Taiyuan University of Technology, Taiyuan, China, in 1986.

She is currently a Professor in the College of Electrical and Power Engineering, Taiyuan University of Technology. Her research interests include electric-machine analysis, design, control, and power electronics.

Yun Ma received the B.Sc. and M. Sc. degrees in electrical engineering from the Taiyuan University of Technology, Taiyuan, China, in 2008 and 2013, respectively.

He is currently working in State Grid Jinzhong Power Supply Company, Jinzhong, China.

Xin Wang received the B.Sc. and M.Sc. degrees in electrical engineering from the Taiyuan University of Technology, Taiyuan, China, in 2009 and 2012, respectively.

She is currently working in CSR Zhuzhou Electric Company, Zhuzhou, China.

Jun Yan received the B.Sc. degree from the Taiyuan University of Technology, Taiyuan China, in 2012, where he is currently working toward the M.Sc. degree in the field of machine control.

Zhizhong Ma received the B.Sc. degree from the Taiyuan University of Technology, Taiyuan China, in 2013, where he is currently working toward the M.Sc. degree in the field of machine control.